TanDepth: Leveraging Global DEMs for Metric Monocular Depth Estimation in UAVs

Horatiu Florea and Sergiu Nedevschi

Abstract—Aerial scene understanding systems face stringent payload restrictions and must often rely on monocular depth estimation for modelling scene geometry, which is an inherently ill-posed problem. Moreover, obtaining accurate ground truth data required by learning-based methods raises significant additional challenges in the aerial domain. Self-supervised approaches can bypass this problem, at the cost of providing only up-toscale results. Similarly, recent supervised solutions which make good progress towards zero-shot generalization also provide only relative depth values. This work presents TanDepth, a practical, online scale recovery method for obtaining metric depth results from relative estimations at inference-time, irrespective of the type of model generating them. Tailored for Unmanned Aerial Vehicle (UAV) applications, our method leverages sparse measurements from Global Digital Elevation Models (GDEM) by projecting them to the camera view using extrinsic and intrinsic information. An adaptation to the Cloth Simulation Filter is presented, which allows selecting ground points from the estimated depth map to then correlate with the projected reference points. We evaluate and compare our method against alternate scaling methods adapted for UAVs, on a variety of real-world scenes. Considering the limited availability of data for this domain, we construct and release a comprehensive, depth-focused extension to the popular UAVid dataset to further research.

Index Terms—Metric Monocular Depth Estimation, Global Digital Elevation Models, Aerial Scene Understanding.

I. Introduction

Recent years have brought constant technical progress and increasing economies of scale in the Unmanned Aerial Vehicle (UAV) market, accelerating research interest [1]. Their roles expand beyond industrial settings like surveying and agriculture to fields of crisis response, such as wildfires [2] or search and rescue [3]. To maximize the reliability and utility of UAVs, advanced perception systems encompassing tasks such as object detection, localization and mapping are being actively developed. A key function of such systems is to generate a consistent, accurate representation of the 3D geometry in the flight area modelling terrain, natural and man-made structures, as well as actors present in the scene.

A variety of scene geometry data sources are available to aerial-based applications, each having particular strong and weak points. Global Digital Elevation Models (GDEM) boast high coverage but are of low horizontal resolution

The authors are with the Department of Computer Science, Technical University of Cluj-Napoca, 400114, Cluj-Napoca, Romania (e-mail: First-Name.LastName@cs.utcluj.ro)

© 2024 IEEE. Personal use of this material is permitted. Permission from IEEE must be obtained for all other uses, in any current or future media, including reprinting/republishing this material for advertising or promotional purposes, creating new collective works, for resale or redistribution to servers or lists, or reuse of any copyrighted component of this work in other works.



Fig. 1. TanDepth enables relative depth maps (left window) used by UAVs for estimating scene geometry to be scaled using sparse points (green) part of a satellite-based Global Digital Elevation Model, yielding metric depth results

and are typically acquired with a low temporal frequency, increasing the possibility of containing outdated data. 3D products obtained through Airborne Laser Scanning (ALS) or image-based photogrammetry processes feature significantly higher resolutions but face the same risk of stale data, in addition to reduced availability. Gaining traction in recent years, Neural Radiance Fields (NeRF) [4] learn to represent a scene's geometry from a set of posed images, but are typically considered an offline solution and face challenges in large scenes. On-board LiDAR scanners can provide real-time, direct depth measurements at the cost of added bulk, synchronization, and calibration requirements. Computational solutions such as Structure from Motion (SfM) and Multi-View Stereo (MVS) use multiple images to estimate depth in real-time, but face challenges on certain textures, or lack thereof.

Detecting and localizing dynamic objects such as pedestrians and vehicles is vital in many applications, yet all methods presented so far face challenges when modelling such objects, ranging from significant (e.g., on-board LiDAR, NERF) to insurmountable (e.g. GDEM, ALS/photogrammetry, SfM). This limitation, in conjunction with others mentioned, makes deep learning based Monocular Depth Estimation (MDE) methods the best candidate solution, with the Single Image Depth Estimation (SIDE) variant being the focus of this paper. As estimating 3D geometry from a 2D view is an inherently ill-posed problem, MDE approaches typically produce lower quality results than other methods, but compensate by being able to provide online results, including for dynamic scene elements. Moreover, fusing additional information such as semantic or panoptic information with MDE-provided geometric data is straightforward, as both are directly derived from the RGB modality.

Recent MDE works [5]–[7] continue to stress the importance of high quality ground truth depth data. Unfortunately, as we highlighted in [8], there are few real-world depth datasets covering outdoor UAV scenarios. Self-supervised MDE methods are being developed as alternatives to supervised learning approaches to lessen the burden on data requirements. These can learn over image sequences without the need for depth ground truth [9], but can only provide relative estimations, with an unknown scale, a limitation inherent to the training process. The same limitation is found in recent depth foundation models Depth Anything [6] and Depth Anything V2 [7] which follow the scale- and shift-invariant (SSI) training procedure proposed in MiDaS [5] in order to achieve high performance in zero-shot generalization across domains. SSI training, like in self-supervision, leads to learning a *relative* depth model, instead of an absolute one. Obtaining metric measurements remains, however, essential in most applications.

We consider robust scale recovery methods to be important milestones towards general metric depth estimation systems, as recent seminal works on relative depth estimation [6], [7] show that decoupling scale during training can lead to impressive gains in generalization performance. Pairing such models, trained on large-scale data, with online scale recovery methods designed for each application domain can enable powerful capabilities.

To further this vision, we propose TanDepth, a novel method which capitalizes on the nearly universal coverage of Global Digital Elevation Models, such as TanDEM-X [10], to generate metric depth maps from relative MDE models in outdoor UAV applications. Our method involves using camera extrinsic and intrinsic parameters to project GDEM data into the camera view, with projected points taking the role of true depth anchors in the subsequent scaling step. Possible occlusions and alignment inaccuracies are handled by performing scaling only using ground surface points. We adapt the Cloth Simulation Filter [11], initially developed for aerial LiDAR scans, to run on 3D data from SSI relative depth estimations in order to segment ground patches, which, to the best of our knowledge, would represent its first use on MDE data. Fig. 1 graphically illustrates the proposal.

In order to validate our method, we conduct experiments on a selection of scenes from 3 public datasets, diverse in terms of visible depth ranges, terrain profiles, vegetation, man-made structures and regional aesthetics. For enabling comparisons, we adapt the existing camera height-based scaling used in automotive applications to outdoor aerial environments, as well as for use with estimations coming from SSI models. Furthermore, we release UAVid-3D-Scenes, an extension to the UAVid [12] dataset, to support future development of the aerial MDE field.

Our contributions presented in this paper can be summarized to:

• TanDepth: A novel online scale recovery method based on Global Digital Elevation Model data that, when paired with modern relative depth estimators, can provide high quality zero-shot metric depth in aerial scenarios, as demonstrated through evaluations across 4 varied scenes from 3 datasets: UAVid [12], UFO Depth [13] and WildUAV [14]. The

- key role scaling has on generalization performance is highlighted through experiments with multiple depth models, including an absolute metric model.
- Through straightforward adaptations, we enable the use of the Cloth Simulation Filter [11] on scale- and shiftinvariant monocular depth estimations for segmenting ground surfaces, outside its designed use on aerial LiDAR scans
- We adapt an existing scale recovery method based on camera height priors to function in outdoor UAV applications with scale- and shift-invariant relative depth maps, in order to compare against our proposed method.
- UAVid-3D-Scenes¹ Dataset: We release an extension for the widely used UAVid [12] dataset, specifically focused on depth estimation and scene reconstruction tasks, that includes RGB, depth, pose and camera intrinsics information.

II. RELATED WORK

Monocular Depth Estimation. Typically framed as a supervised regression task, some of the recent advancements in MDE focus on the underlying network architecture [15], integrating camera model knowledge [16], [17] and optimizing learning over collections spanning multiple datasets [5]–[7], typically disentangling scale and providing relative estimations. Other lines of work focus on recasting MDE as a classification task in the form of an ordinal regression network to exploit more favorable learning traits [18]–[20]. This approach is proposed even solely for the task of relative to metric scaling [21]. Some works targeting UAVs refine the ordinal regression for longer ranges [22] or by using semantic guidance [23] while others propose learning from virtual stereo pairs [24] or reuse previous estimations [25]. Self-supervised MDE approaches [9], [26]–[28] aim to lessen the need for annotated data during training by framing the task in the context of novel view reconstruction problems, where supervision is derived from photometric inconsistencies between real and reconstructed frames, with some works tackling the aerial domain as well [29], [30].

Scale Recovery Methods. Relative MDE models, irrespective of the training methodology employed, require additional subsystems in order to provide metric measurements. In the automotive domain, these can exploit information on the known, fixed camera height [31], [32] or even auxiliary Radar data [33] to perform scaling. Some works propose learning scale during training, through direct supervision with pose information [34] or using an auxiliary scale network trained on synthetic data with dense ground truth [35]. In aerial environments, [36] use depth computed analytically from dense optical flow and GPS-based odometry data to scale estimations from a selfsupervised model in order to build a pseudolabeled dataset that is later used to distil knowledge to a student model. Similar to works in automotive scenarios, [37] scale depth estimations by using the UAV's height above the ground, as measured by a downward facing Time of Flight (TOF) sensor. However, the

¹The UAVid-3D-Scenes data, example code and further details will be made available on the project's GitHub page

approach is limited to mainly indoor applications, due to the TOF sensor's limited range and to depth models that are scaled using a single multiplicative term.

Global Digital Elevation Models. Rapid advancements in space-based remote sensing capabilities have enabled the creation of 3D GDEMs that provide almost complete coverage of the Earth's surface. GDEM data is already used in UAV applications to enable terrain-aware mapping functions that keep flight altitude constant relative to the mapped area. Technological advances have led to GDEMs boasting higher accuracy and resolution over time: the Shuttle Radar Topography Mission (SRTM) [38] used Synthetic Aperture Radar (SAR), while the ASTER [39] and JAXA ALOS 3D [40] GDEMs used image-based stereoscopic reconstructions. For our work, we selected to use the TanDEM-X 30 m Edited DEM which was recently released publicly. The data is part of the TanDEM-X [10] project, which uses the first space-based bistatic SAR system comprised of two near-identical satellites, providing measurements with vertical accuracy better than 2 m, homogeneously across all land masses.

Aerial Datasets. Capturing high quality datasets representative for outdoor aerial perception tasks poses unique and complex challenges. Synthetic data generation solutions such as AirSim [41] can be used to develop datasets such as Mid-Air [42] or TartanAir [43], leaving open the issue of addressing the synthetic-to-real domain gap. While RGB, pose and even semantic data can be obtained in a straightforward manner, capturing aerial ground truth depth maps is cumbersome and is tackled by few works. The WildUAV [14] dataset is one of the first collections providing photogrammetry-based ground truth depth and pose data for outdoor aerial nadir and oblique images. UFO Depth [13] makes available oblique UAV video collections together with accurate pose data which enable reconstructing the 3D scene. Recently released, the UseGeo [44] dataset provides nadir images alongside LiDAR-based depth maps captured from a UAV. While only providing semantic annotations, the UAVid [12] oblique video dataset is noteworthy due to its wider adoption.

III. METHOD

A. Scale Recovery Methods for Aerial MDEs

Traditional offline evaluation procedures for relative depth models include a scaling pre-processing step to ensure the arbitrary scale predictions match the scale (typically metric) of the ground truth depth maps D^* used for evaluation. Commonly, MDEs infer disparity d, which is converted to depth values as D=1/d. The standard depth scaling procedure computes a linear scale factor sf between the median values of the two depth maps $sf=\mathrm{median}(D^*)/\mathrm{median}(D)$, which is then used to scale the predictions as: $\bar{D}=sf*D$. Naturally, such a strategy is inapplicable to any online, real-world application, due to unavailability of the GT data.

The trivial online solution for scaling predictions is to precompute a series of scaling factors on frames from validation dataset (with known GT) and then use the average (or median) value from the series as a fixed scaling factor ($sf_{\rm fixed}$) during online operation. Clearly, this method assumes that the model's

predictions exhibit scale consistency over varying datasets and conditions, which is not typically the case (especially for self-supervised models) and is an active research topic [45]. Scale inconsistencies can be even more pronounced in aerial scenarios in which flight parameters (altitude, camera pitch, etc.) can vary and significantly modify the scene geometry in the frame. For more details on the standard scaling procedure, we direct readers to consult monodepth2 [27].

$$\hat{d} = \frac{d - t(d)}{s(d)} \tag{1}$$

$$s(d) = \frac{1}{M} \sum_{i=1}^{M} |d - t(d)| \qquad t(d) = \text{median}(d)$$
 (2)

The standard scaling procedure requires further adaptation for models (such as DepthAnything [6]) trained using the scale- and shift-invariant loss, first proposed by MiDaS [5]. This training strategy aligns both the prediction and the ground truth disparity maps to have zero translation and unit scale, before computing the mean-squared error loss. For a disparity map d of size M, the scale- and shift-invariant map \hat{d} is obtained using Eq. 1, where the scale and shift terms are computed according to Eq. 2. In order to realign a prediction \hat{d} generated by such a model to the ground truth d^* , one can employ a closed-form solution of the least-squares criterion presented in Eq. 3. This computes the scale and translation terms which are used to scale the prediction as $\bar{d} = s\hat{d} + t$. This scaling procedure is compatible with other types of relative MDEs, such as those trained using self-supervision.

$$(s,t) = \underset{s,t}{\operatorname{argmin}} \sum_{i=1}^{M} (s\hat{d}_i + t - d_i^*)^2$$
 (3)

Online use of this approach is hampered by its dependency on the ground truth map d^* . We thus aim to find a suitable replacement that accurately captures the scale of the observed scene. First, we present an adaptation of camera height-based methods [31] that enables them to operate on scale-invariant depth maps, by replacing d^* in Eq. 3 with h^* , computed based on known height and camera pitch. This is followed by our proposed method, TanDepth, which computes a sparse metric ground map \tilde{g}^* from GDEM data which more accurately captures the local scene's geometry.

B. Adapting Camera-height Scaling for Scale-invariant MDEs

The authors of [31] present a scale recovery method designed for automotive applications, where cameras are typically placed at fixed, known heights on the vehicle's body. This prior is exploited to compute a scaling factor which places the road surface detected in the depth map at the correct height, thus scaling the results of the self-supervised model. We adapt this method for both the aerial domain and for scale and shift invariant models in order to use it as a benchmark of scaling performance.

Estimated depth information is first back-projected to 3D space using camera intrinsics, after which, in aerial scenarios, the ground surface must be aligned to the XY-plane, by rotating

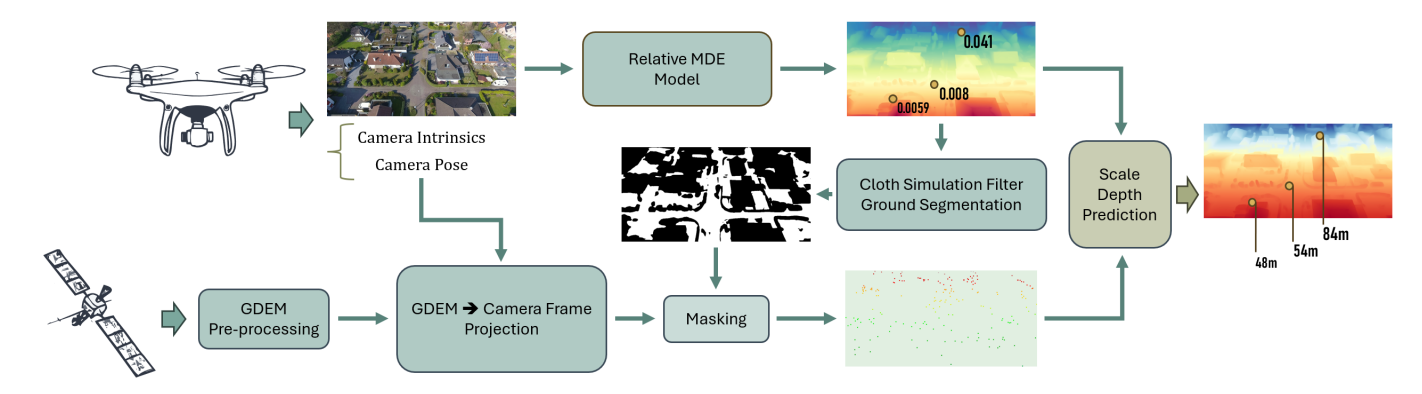


Fig. 2. TanDepth processing flow. RGB, pose, intrinsics and GDEM inputs are processed to generate a sparse metric ground map which is used to scale a relative depth map estimated by a MDE model. The unscaled depth is used to generate a ground segmentation that masks out any GDEM points projected from other surfaces

the cloud to compensate for the camera pitch angle. The fixed height prior must also be adapted for use in UAVs, by replacing it with a dynamic Above Ground Level (AGL) value $h_{\rm agl}$. This can be provided directly by devices such as Radar altimeters or can be computed based on the true Mean Sea Level (MSL) altitude and a DEM of the flight area. Surface normals are computed for all depth map pixels in order to select ground points gp_i (with normals close to ideal ground normal). In our implementation we augment the selection by subsequent filtering using CSF segmentation (see Section III-C3). For each selected ground point, its height h_{gp}^i can be retrieved as the vertical axis component in the back-projected, pitch-aligned 3D point cloud.

Originally, the scaling factor sf is computed by correlating the median ground point height with the known camera height as: $sf = h_{\rm agl}/{\rm median}(h_{gp})$. This works for self-supervised models, but fails for scale invariant ones, as replacing the inferred, invariant disparity \hat{d} with its corresponding height map h_{gp} (and d^* with $h_{\rm agl}$) in Eq. 3 leads to the naive solution $(s=0,t=h_{\rm agl})$, which cancels out the inferred disparity. To solve this and enable the method's use with a larger variety of depth models, we propose performing the scaling operation directly in the disparity space of the network's output instead of the height space.

Our adaptation builds a height-based disparity map h^* that models the ground as a flat planar surface. For each row r in h^* we compute the distance a ray passing through r travels until intersecting the ground. This can be computed as $dist_r = h_{\rm agl}/cos(\alpha_r)$, where α_r is the angle of the ray relative to the ground, taking into account camera pitch and Field of View (FoV) – an angle of 0° corresponds to rays parallel to the ground plane, while those orthogonal feature an angle of 90° . The h^* map, containing disparities corresponding to each row's $dist_r$, replaces the ground truth disparity map d^* in Eq. 3, yielding (s,t).

C. TanDepth

Our proposed scale recovery method aims to solve the principal limitation of the camera height-based method in aerial scenarios, namely its simplified modelling of the ground as a single planar surface. While this operational assumption

is valid in automotive applications where the camera moves closely above the road surface, this is not the case for UAV operations. Another key difference between automotive and aerial scenarios which affects camera height based methods is the distance to the closest ground points that are visible in the frame. The distance, typically very short in driving applications, is strongly correlated with height, focal length and pitch angle. Larger distances can lead to inaccurate use of the AGL data, which is measured (or computed) directly under the UAV.

TanDepth addresses all such limitations by integrating Global Digital Elevation Model data as a low resolution geometric model of the observed scene. Using camera pose information and intrinsic calibration, GDEM data is projected to the image frame, serving as a terrain-aware prior generated specifically for the current viewpoint. More specifically, we compute a sparse ground map \tilde{g}^* where each pixel i to which a GDEM point is projected stores the disparity g_i corresponding to the Z-axis distance to the point. This map can replace the ground truth map d^* in Eq. 3 and be used to determine the factors (s, t). The method is comprised of a pre-processing step which prepares the DEM data, followed by the occlusion-aware projection to the frame and the masking of non-ground pixels using a ground segmentation based directly off the inferred 3D data, all detailed in the following sections and illustrated in the block diagram in Fig. 2.

1) Pre-flight Setup: As our system operates with metric values, we first reproject the TanDEM-X data from its original WGS84 coordinate reference system (CRS) to the Universal Transverse Mercator zone corresponding to the flight location (e.g. UTM Zone 32N for UAVid Germany data). Coordinates are also translated using a global shift vector in order to reduce errors caused by large numerical values on the XY axes. In our tests, all pre-processing steps were performed using the QGIS [46] and CloudCompare [47] open-source software suites.

In cases where the UAV (or dataset, in case of offline processing) does not provide its WGS84 altitude data, an additional Altitude Sync step must be performed in order to correlate heights relative to the take-off location with the vertical datum of the GDEM. This is done by recording the altitude of the horizontally closest point in the GDEM to the position of the drone while stationary on the ground. This





Fig. 3. TanDEM-X GDEM Projection. Example of GDEM points projected to the image. Left frame shows points from the densified GDEM, right shows raw points from TanDEM-X; in both cases, non-ground points are masked out

vertical shift value can then be added to the altitude reported by the UAV during flight.

During our tests we found the sparseness of TanDEM-X can negatively impact the scaling performance, as, depending on camera height and pitch, only a few points are visible in the image, with some placed on non-ground surfaces. To mitigate this, we densify the GDEM data by first computing a Delaunay 2.5D triangulation on the original points followed by randomly sampling a new point cloud off it. We use a sampling density of $0.05 \,\mathrm{pts/m^2}$ (an ablation study for this value is presented in section IV-C). A comparison of projections based on the densified and original GDEM data is shown in Fig. 3. An alternative method would involve performing the densification using only ground GDEM measurements, to ensure even higher accuracy. As the classification of the points is not known ahead of time, this strategy would have to take place after points are projected to image frame and non-ground points are rejected based on the ground segmentation. This, however, would bring about several limitations: added online computational overhead for interpolating in 3D space and a second round of projections, the risk of few or no initial GDEM points to interpolate from and the possibility of ignoring true ground points which are occluded by other structures.

2) Occlusion-aware GDEM Data Projection: First, the camera's extrinsic parameters R_c, T_c are used to transform the GDEM points from world coordinates to the local camera coordinate system, after which the intrinsic matrix K is used to project them onto the image plane. Points with positive Z distance in the camera coord. sys. and which are mapped inside the image bounds are kept, and their Z coordinate is stored in the sparse map \tilde{g}^* which will be used in the scaling process. Conflicts in which multiple points are mapped to the same pixel are resolved by keeping only the closest, occluding measurement.

This approach cannot solve all occlusion cases due to the sparseness of the GDEM data, even after densification – points belonging to surfaces occluded in the image can still be projected if not directly behind another point from the occluding surface. Comprehensive solutions for this hidden point removal problem are available [48], yet we opted for a simpler solution in our implementation as only a rough filtering is sufficient for the scaling task: a projected point g_i is marked as occluded and discarded if the difference between it and any of its neighbors

in a window W is greater than a threshold th_{occ} . We adapt this approach for aerial views by selecting a wider aspect ratio for W ($h=w\div 2, w=7$ in our tests) and a depth aware threshold $th_{occ}=0.04*g_i$, as the viewpoint typically makes depth values more consistent across (non-occluded) image rows and the magnitude of depth discontinuities increases with distance.

Before using the sparse metric ground map \tilde{g}^* in Eq. 3, it must be constrained to feature only true ground points within the depth range of interest. To this end, we use two masks: a 2D ground segmentation mask M_{CSF} computed using the Cloth Simulation Filter and a range mask M_{Rng} which masks out points outside the target depth range, similar to how ground truth depth maps are masked in standard evaluation practice. Finally, as the scale and shift computation takes place in disparity space, the depth values in \tilde{g}^* are inverted.

3) Adapted Cloth Simulation Filter for Scale-invariant Ground Segmentation: Natural and man-made surface features can negatively impact the vertical accuracy of TanDEM-X data [49]. Such features can also affect the projection and scaling process, through occlusions and outdated structures in the scene. To address this, our scaling solution rejects any non-ground or occluded GDEM points by using a segmentation of visible terrain patches in the input image. This could be provided by a deep learning based semantic segmentation model, which would however add significant costs in terms of data and training complexity. To avoid this, we select the Cloth Simulation Filter [11] (CSF) method for the segmentation task, which was first developed for extracting DTMs from airborne LiDAR data. It works by covering an inverted copy of the 3D scene with a simulated cloth and using its interactions with the 3D points to model the terrain surface and segment the point cloud (PC).

One of CSF's strengths is the relatively low number of parameters requiring tuning, compared to other computational methods. In our system's case however, adapting the cloth resolution and class threshold parameters to each frame represents a challenge, as their values are expressed in the same units as the input point cloud. As the initial PC has an unknown scale, this creates a circular dependency, made worse by the significant warping of PCs obtained from scale-invariant MDE networks.

To solve this, we propose a straightforward adaptation that enables the use of the Cloth Simulation Filter for segmenting







Fig. 4. CSF Ground Segmentation. Results of the ground segmentation based on adapted CSF, overlayed as a turquoise layer over input images from Chilia, Germany and Oveselu scenes, respectively.

ground patches from MDE-generated inputs. As CSF operates on 3D point clouds, the disparity inferred by the network must first be converted to depth measurements, which are then back-projected to 3D space using the inverse intrinsic matrix, K^{-1} . In order to reduce warping inherent to scale-invariant estimations, we perform an initial scaling using a pair of fix parameters, \bar{s} and \bar{t} computed ahead of time on a validation dataset. Using the two parameters and Eq. 3, we are able to compute a rough estimation for a metric depth map, denoted \bar{D} . This initial scaling can be skipped for other types of relative depth models.

$$D_{central}^* = \frac{h_{\text{agl}}}{cos(\text{pitch}_{\text{cam}})} \tag{4}$$

$$\overline{D}_{central} = \text{centralRowsMedian}(\overline{D})$$
 (5)

$$cf = \frac{D_{central}^*}{\overline{D}_{central}} \tag{6}$$

While simple, scaling using the fixed values can produce poor results, especially if the target scenario differs significantly from the one in the validation set used to compute the values. As such, we introduce a secondary refinement step which computes the cf adjustment factor value based on the camera pitch and above ground height (which can be derived from GDEM data). Specifically, we use the two data points to estimate the distance $D_{central}^*$ to a simulated planar ground surface from the central image pixel (Eq. 4, similar to how we build h^* in Section III-B). This value is then used to compute cf by dividing it to the median depth value in the central rows of the rough depth map \overline{D} (Eq. 6; we use 7% of the total number of rows).

Finally, the CSF algorithm can be applied on the point cloud back-projected from \overline{D} , using the parameters 1.5/cf and 0.5/cf for the cloth resolution and class threshold, respectively. For UAVid Germany, we use alternate values of 0.5/cf and 1.25/cf, better suited for the more cluttered scene. As each depth map pixel has a correspondent in the 3D point cloud, it is trivial to convert the CSF output into a 2D segmentation mask,

 M_{CSF} , which is then used to reject any GDEM points projected onto or behind of non-terrain image patches. Examples of generated masks are depicted in Fig. 4.

D. The UAVid-3D-Scenes Dataset

To enable further development of the aerial MDE field, we release a depth-centric extension to the UAVid [12] dataset we name UAVid-3D-Scenes. We release a total of 5517 samples for which the undistorted RGB image and the depth map image is provided. Out of these, 2985 frames (sampled from videos at rates of 2 and 5 FPS in Germany, 2 FPS in China) have an associated dense depth label C generated using the MVS reconstruction stage of COLMAP [50], [51], while the rest (sampled at 2 FPS) feature sparse depth labels C^{\ast} . The assets are provided at a resolution of $512 \times 1024 \mathrm{px}$.

Originally, the UAVid [12] dataset was released as a collection of 42 fixed length (901 frames) video sequences, 9 of which were recorded in Germany and the rest in China. We rearrange the sequences in order to perform the 3D reconstructions at *scene* level, where a scene can be composed of one or more sequences recorded over the same area. This adds more context to the data and can help the reconstruction through loop closures. We thus group the original sequences into 12 scenes.

As other works have noted [29], the Germany and China subsets exhibit core differences in terms of scene content and even recording parameters, impacting the performance of 3D reconstruction tasks. As such, dense reconstructions were successful for both scenes in Germany, while the large number of dynamic elements in China allowed only one scene to be densely reconstructed. The challenging conditions affected the sparse reconstructions as well, prompting us to manually clean-up the point clouds, in addition to using the Statistical Outlier Removal filter in CloudCompare [47]. Examples of the dense and sparse reconstructions are depicted in Fig. 5 – dark blue pixels represent patches lacking depth information.









Fig. 5. UAVid-3D-Scenes. Examples of the dense (left) and sparse (right) depth reconstructions for UAVid scenes recorded in Germany and in China, respectively.

Scene	Scaling	Lower is better ↓			Higher is better ↑						
		AbsRel	SqRel	RMSE	LogRMSE	δ_1	δ_2	δ_3	$ar{\delta}_1$	$\bar{\delta}_2$	$\bar{\delta}_3$
UAVid Germany	Fixed	0.062	0.424	4.693	0.072	0.983	0.999	1.000	0.265	0.494	0.714
	Cam. Height	0.039	0.262	3.854	0.055	0.988	0.999	1.000	0.519	0.763	0.878
	ZoeDepth*	0.041	0.218	3.659	0.054	0.992	0.999	1.000	0.358	0.720	0.899
	TanDepth	0.031	0.143	2.800	0.044	0.993	1.000	1.000	0.523	0.863	0.944
	GT	0.027	0.133	2.720	0.041	0.994	1.000	1.000	0.654	0.879	0.938
UFO Depth Oveselu	Fixed	0.218	6.966	25.147	0.290	0.485	0.800	0.972	0.076	0.148	0.213
	Cam. Height	0.112	2.097	12.233	0.124	0.885	0.996	1.000	0.184	0.336	0.462
	ZoeDepth*	0.171	2.933	14.866	0.185	0.707	0.998	1.000	0.069	0.140	0.212
	TanDepth	0.048	0.344	5.498	0.061	0.997	1.000	1.000	0.330	0.592	0.784
	GT	0.040	0.285	5.057	0.053	0.997	1.000	1.000	0.430	0.701	0.849
	Fixed	0.425	28.214	67.528	0.614	0.036	0.295	0.680	0.001	0.002	0.004
LIEO Daniel	Cam. Height	0.052	0.675	9.078	0.066	0.991	0.999	1.000	0.347	0.602	0.774
UFO Depth Chilia	ZoeDepth*	0.116	3.072	23.232	0.151	0.850	0.998	1.000	0.095	0.201	0.319
	TanDepth	0.040	0.442	7.520	0.055	0.994	0.999	1.000	0.427	0.715	0.872
	GT	0.035	0.362	7.064	0.049	0.995	0.999	1.000	0.496	0.779	0.904
	Fixed	0.345	7.052	18.334	0.304	0.295	0.913	0.997	0.007	0.015	0.026
WildUAV	Cam. Height	0.207	9.483	10.981	0.178	0.828	0.959	0.966	0.116	0.230	0.345
	ZoeDepth*	0.502	14.876	27.551	0.415	0.062	0.673	0.977	0.001	0.001	0.003
	TanDepth	0.072	1.269	4.106	0.085	0.962	0.996	0.997	0.322	0.531	0.670
	GT	0.041	0.157	2.560	0.052	0.995	1.000	1.000	0.448	0.708	0.846

DEPTH ANYTHING [6] WITH DIFFERENT SCALING APPROACHES. TANDEPTH OUTPERFORMS FIXED AND CAMERA HEIGHT ONLINE SCALING METHODS ACROSS THE TESTED DATASETS (BEST RESULTS IN BOLD), APPROACHING THE PERFORMANCE OF OFFLINE GROUND TRUTH SCALING (IN ITALIC).

ZOEDEPTH IS A METRIC DEPTH ESTIMATION MODEL TRAINED ON UAVID

We additionally provide camera extrinsic (pose) data for each sample along with camera intrinsics, both obtained through the sparse SfM reconstruction process. Metric scaling of the reconstructed models is derived differently for the two locations: in Germany scale and global position was recovered by aligning the reconstructions with public aerial LiDAR 3D scans (using Iterative Closest Point), while for China the scale was recovered by manually correlating sizes of various landmarks (roads, buildings, etc.) between the reconstructions and map data.

As part of their work on self-supervised MDE for aerial environments the authors of [29] have released a small subset (3 sequences) of depth reconstructions for the UAVid [12] dataset, under the name of UAVid-Depth. Our proposal differs both in scope (covering the entire UAVid dataset [12]) as well as in terms of contents (providing camera intrinsics, depth maps as well as pose information at scene level, with global position estimations for the German sequences).

IV. EXPERIMENTS

A. Datasets, Evaluation & Implementation Details

We use Depth Anything [6] as the baseline relative depth model using its default inference setup, as we consider it an ideal representative for relative MDE models with strong generalization capabilities. All tests are performed at the 512×1024 resolution (both input image and ground truth depth map) on undistorted images. The evaluation ground truth depth maps were generated using the dense reconstruction pipeline in COLMAP [50], [51]. The TanDEM-X [10] Global Digital Elevation Model used in the scale recovery process was interpolated to a density of $0.05\,\mathrm{pts/m^2}$. The code was developed in Python and uses the official implementation of the Cloth Simulation Filter for the language.

For evaluating TanDepth we employ 542 frames from the proposed UAVid-3D-Scenes dataset, part of the captures in Germany which feature a flat terrain profile. From the UFO Depth [13] dataset, we use the Chilia (flat terrain, 301 frames) and Oveselu (hilly terrain, 299 frames) scenes in the evaluation for which we perform dense 3D reconstructions using COLMAP [50], [51] that are then scaled by aligning the reconstructed poses with the corresponding GPS data. From WildUAV [14], we use 265 oblique images from the hilly "scene1" capture. Evaluation is carried out for the 30 m to 150 m range which covers most of the frame for these captures, with an extended range of 50 m to 250 m range used for Chilia, where the shallower pitch angle leads to longer in-frame distances. Global positioning information for each frame was directly available for UFO Depth [13] and WildUAV [14], while for UAVid [12] Germany it was recovered through registration with public aerial LiDAR scans of the area (see Section III-D).

Training an absolute depth model can be an alternative to a system combining a relative model with an online scale recovery method. This involves using a supervised learning approach on sufficient (-ly diverse) metric ground truth data, a difficult task for aerial tasks. To further evaluate the effectiveness of our proposed scaling method, we want to compare its performance with a metric depth model adapted for the aerial domain, following the same recipe proposed in [6] for the automotive and indoor domains.

Specifically, we use ZoeDepth [21] to train a depth decoder and metric bins module on top of the Depth Anything [6] pre-trained encoder, in order to obtain absolute depth estimations. We train the system for aerial environments using only sparse labels generated for both China and Germany scenes. As this model directly produces absolute estimations, no post-inference scaling is required, but it is included in our study as an alternate option to TanDepth for absolute depth systems. The standard training settings are used for training, which is carried out on a set of 3400 frames for 20 epochs.

We compute and report the widely adopted error metrics of Absolute Relative Error (AbsRel), Square Relative Error (SqRel), Root Mean Square Error (RMSE) and Root Mean Square Log Error (LogRMSE), as well as the Threshold Accuracy metrics $\delta < 1.25^T$, where $T \in 1, 2, 3$ and $\delta = \max(D^*/D, D/D^*)$. It can be observed in Table I that this

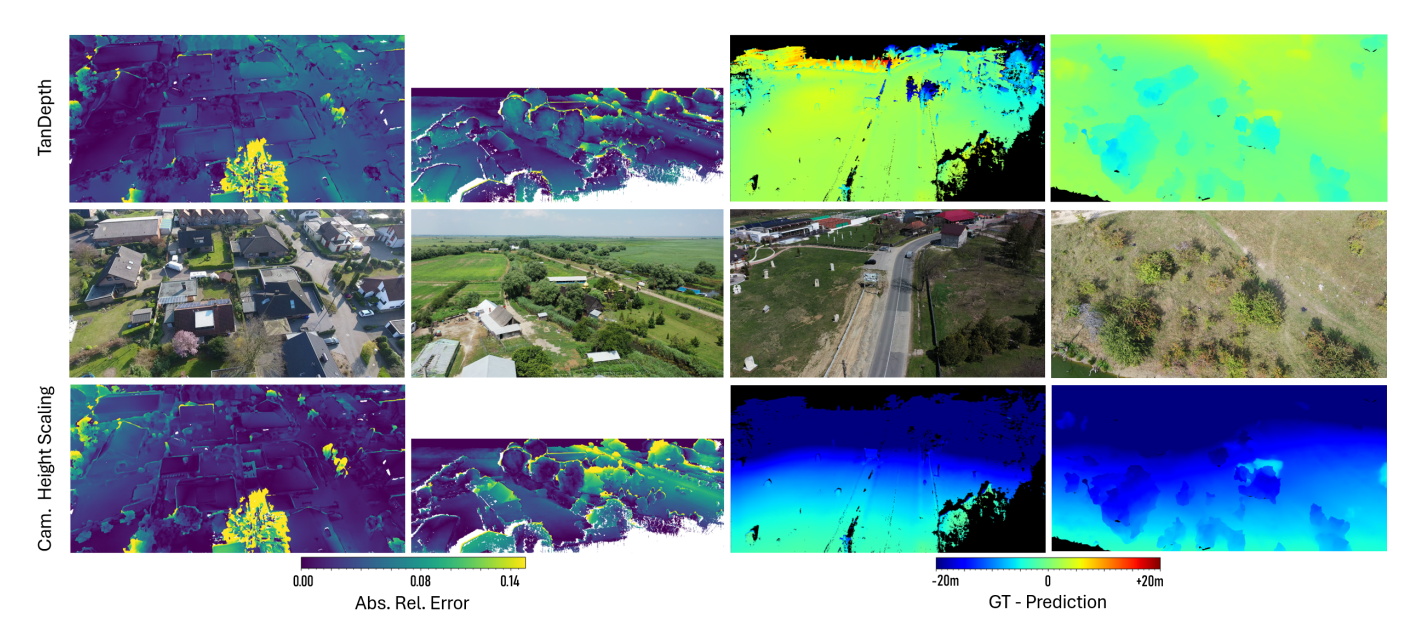


Fig. 6. TanDepth Qualitative Results. First two columns: absolute relative error maps for frames in UAVid and UFO Depth Chilia. Last two columns: Error maps depicting signed difference between ground truth and scaled predictions, in UFO Depth Oveselu and WildUAV. Top row features predictions scaled with TanDepth, while the bottom row shows scaling using method based on camera height.

metric is close to saturation in the aerial domain, as δ^1 allows, for example, errors of up to $12.5\,\mathrm{m}$ (25%) for points at $50\,\mathrm{m}$. To improve relevance, we propose a tenfold decrease of the threshold: $\bar{\delta} < 1.025^T$.

B. Absolute Depth Estimation using TanDepth Scaling

Table I reports results for the proposed TanDepth scaling method in comparison with alternate strategies for generating metric depth results starting from a relative MDE. Tested scaling methods include using fixed scaling factors precomputed on a validation set (in our case, on the UAVid Germany Val set), using camera height-based scaling adapted for UAVs (Cam. Height), the trained ZoeDepth metric model and the reference, evaluation-only strategy of scaling each frame with its corresponding ground truth (GT) depth map.

The quantitative evaluation highlights significant improvements the proposed scaling methods consistently brings, across all tested datasets, building towards closing the gap between online methods and the offline reference, GT scaling. Fixed factor scaling is typically the worst performer, as one would expect, as the network's outputs skew away from the distribution observed on the validation set used for computing the scalars. The performance of camera height-based scaling significantly drops, as predicted, for environments featuring uneven, hilly terrain, such as UFO Depth Oveselu and WildUAV, compared to the other, flat areas. Learning to directly infer metric depth, although specifically trained on aerial domain data (UAVid) and starting from the same powerful encoder (Depth Anything [6]), shows its generalization limitations, through poor results on outof-distribution data (UFO Depth, WildUAV). This comes in line with challenges observed for the UniDepth [17] metric MDE, tested in Sect. IV-C which performs poorly outside its target automotive domain. Moreover, the performance degradation on out-of-distribution evaluations we observe for ZoeDepth in

Scene	Filter	AbsRel↓	SqRel↓	RMSE↓	$\bar{\delta}_1\uparrow$	$\bar{\delta}_2\uparrow$	$\bar{\delta}_3 \uparrow$
UAVid	None	0.044	0.250	3.648	0.365	0.756	0.890
Germany	Sem.	0.030	0.142	2.801	0.577	0.867	0.942
(Semantic)	CSF	0.031	0.144	2.809	0.542	0.869	0.943
UFO Depth	None	0.055	0.405	5.788	0.291	0.543	0.733
Oveselu	CSF	0.048	0.344	5.498	0.330	0.592	0.784
UFO Depth	None	0.075	1.227	10.617	0.276	0.475	0.625
Chilia	CSF	0.040	0.442	7.520	0.427	0.715	0.872
			TABLE II				

GROUND SEGMENTATION ABLATION STUDY. MASKING OUT NON-GROUND PATCHES WITH THE CLOTH SIMULATION FILTER-BASED SEGMENTATION IMPROVES TANDEPTH PERFORMANCE. ON A SUBSET OF FRAMES IN UAVID GERMANY FOR WHICH SEMANTIC ANNOTATIONS ARE PROVIDED, THE PERFORMANCE OF THE TWO SEGMENTATION TYPES IS SIMILAR.

the aerial domain is comparable to that observed by others in the automotive context [6], [21].

Qualitative results using TanDepth and camera height-based scaling are illustrated in Fig. 6. These confirm that the proposed method handles sloped scenes (last two columns) significantly better than the height based approach, which tends to flatten elevations further downfield (predicted value is greater compared to true depth). For flatter scenes, the differences between the two are comparable. Another aspect to note are errors around large vegetation, appearing due to differences in how the depth model and the multi-view-stereo method used to generate the ground truth reconstruct such objects.

To validate TanDepth's applicability to online systems, we measure the average execution times for the proposed components. The test was conducted without GPU acceleration on an Intel Core i7-6700K CPU, using the official Python wrapper for the CSF algorithm, without parallelism or other advanced optimizations, which are beyond this paper's scope. Evaluation was carried out on the UFO Depth [13] Oveselu scene, using a $4.8\,\mathrm{km^2}$ GDEM tile. Projecting the GDEM points took, on average, $2.5\,\mathrm{ms}$, the occlusion handling pass took $268\,\mathrm{ms}$ and the Cloth Simulation Filter another $253\,\mathrm{ms}$.

Scene	Model	Scaling	AbsRel↓	SqRel↓	RMSE↓	$\bar{\delta}_1\uparrow$	$\bar{\delta}_2\uparrow$	$\bar{\delta}_3\uparrow$
	Depth Anything	GT	0.040	0.285	5.057	0.430	0.701	0.849
	Deput Anything	TanDepth	0.048	0.344	5.498	0.330	0.592	0.784
UFOD	Depth Anything V2	GT	0.042	0.311	5.252	0.426	0.682	0.829
Oveselu		TanDepth	0.051	0.380	5.726	0.309	0.567	0.757
Oveseiu		None*	0.581	32.957	56.982	0.000	0.000	0.001
	UniDepth	GT	0.040	0.282	5.180	0.424	0.703	0.847
		TanDepth	0.047	0.310	5.233	0.326	0.607	0.797
	Donth Anything	GT	0.035	0.362	7.064	0.496	0.779	0.904
	Depth Anything	TanDepth	0.040	0.442	7.520	0.427	0.715	0.872
UFOD	D 4 4 41 170	GT	0.033	0.328	6.661	0.521	0.811	0.922
	Depth Anything V2	TanDepth	0.039	0.410	7.206	0.424	0.736	0.888
Chilia		None*	0.513	43.361	84.116	0.001	0.002	0.004
	UniDepth	GT	0.040	0.440	7.905	0.440	0.716	0.859
		TanDepth	0.046	0.517	8.122	0.386	0.653	0.815
	D 41 - A 41 - 1	GT	0.041	0.157	2.560	0.448	0.708	0.846
	Depth Anything	TanDepth	0.072	1.269	4.106	0.322	0.531	0.670
	D d A d: 170	GT	0.043	0.180	2.763	0.427	0.686	0.830
WildUAV	Depth Anything V2	TanDepth	0.106	2.510	5.723	0.254	0.431	0.552
		None*	0.353	6.908	18.958	0.000	0.001	0.002
	UniDepth	GT	0.048	0.240	3.396	0.351	0.625	0.798
	•	TanDepth	0.159	3.860	12.016	0.175	0.305	0.404
		•	TABLE III					

MDE MODEL COMPARISON. FOR EACH METRIC, THE BEST RESULT IS IN BOLD, PER SCENE. UNIDEPTH IS AN ABSOLUTE (METRIC) DEPTH MODEL, YET ITS PERFORMANCE ON AERIAL SCENES IS QUITE POOR PRIOR TO APPLYING A SCALING APPROACH.

C. TanDepth Ablation Studies

Effect of Ground Segmentation. We perform experiments to measure the effect ground segmentations have on the quality of the scaled estimations. First, we evaluate the proposed CSF-based filtering which can be applied directly on the initial (unscaled) depth, comparing it with evaluations in which no ground filtering is applied, over three scenes. In addition, on UAVid Germany, we use available semantic annotations to compare how a semantic model-based segmentation would perform for the filtering task. To obtain a similar ground segmentation from the semantic image, we select pixels classified as either "Road" or "Low Vegetation", the two UAVid classes which encompass the majority of ground points. Note that for this test, we use only frames for which semantic annotations are available, which would be used to train the segmentation model and represent an ideal segmentation.

The results presented in Table II confirm that limiting the scaling process to using only ground patches in the observed camera frame leads to improvements in the resulting depth estimation. At the same time, using the semantic annotations leads to similar scaling performance, despite relying on more complex data.

MDE Model Comparison. Table III presents results comparing the performance of three state of the art MDE models in the aerial context. Each model is evaluated both using ground truth scaling, as well as in conjunction with the proposed TanDepth approach. As a metric MDE model, we additionally evaluate UniDepth [17] without any type of scaling running it with provided camera intrinsics.

The two versions of Depth Anything behave similarly, with the first version outperforming the second one in two of the tested scenes. Without scaling, UniDepth's excellent zero-shot performance in the automotive domain, for which it was designed, does not translate well to aerial viewpoints. However, by evaluating it in conjunction with an additional scaling mechanism, its performance dramatically ameliorates, supporting the view that limitations in MDE generalization are strongly linked with the issue of scale.

Points/m ²	AbsRel↓	SqRel↓	RMSE↓	$\bar{\delta}_1 \uparrow$	$\bar{\delta}_2\uparrow$	$\bar{\delta}_3\uparrow$			
Original	0.051	0.374	5.676	0.323	0.581	0.765			
0.005	0.049	0.354	5.561	0.326	0.586	0.776			
0.05	0.048	0.344	5.498	0.330	0.592	0.784			
0.5	0.049	0.352	5.559	0.329	0.593	0.783			
TARLE IV									

Densification Ablation. Comparing the effects of different GDEM Densification strengths on UFO Depth Oveselu scene. The $0.05~{\rm pts/m}^2$ value is the default used throughout the other experiments in the paper.

Depth Anything V2 [7], as the successor of Depth Anything [6], inherits many of its advantages while better preserving fine details. This can be clearly observed in the qualitative comparison between the two, in Fig. 7, such as for the construction crane in the first image. Of interest for aerial applications is also V2's improved handling of reflective water surface, such as those in the second image (below top right skyscrapers). The level at which the model is able to resolve fine details at significant distances is impressive, and highlights the limitations of standard quantitative evaluation metrics which don't capture such differences.

Effect of GDEM Densification. A separate experiment, presented in Table IV was conducted on the UFO Depth Oveselu scene to evaluate the impact of GDEM data density has on the scaling performance. The default density value of $0.05\,\mathrm{pts/m^2}$ used in all of the presented experiments in the paper is compared with two other values, as well as to using the original GDEM data directly. While the performance deltas are limited in magnitude, increasing the density of the data is shown to improve the scaling performance. Of note is that higher densities also reduce the number of frames for which scaling can't take place due to lack of projected ground GDEM points. At the same time, increasing the GDEM density inherently increases the number of projections and thus, computational complexity.

V. CONCLUSION

In this work, we present TanDepth, a practical online scale-recovery approach for monocular depth estimation that

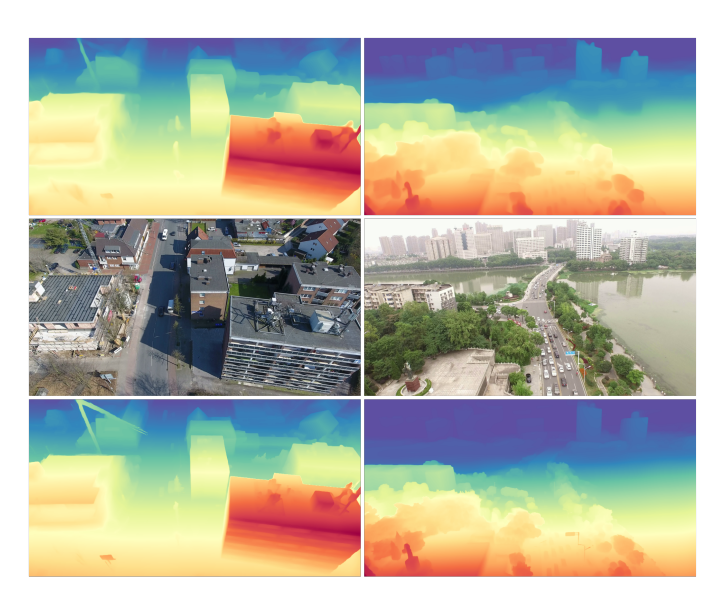


Fig. 7. Qualitative comparison of disparity maps generated by Depth Anything V1 (1st row) and V2 (3rd row) on aerial data. V2's training setup clearly improves fine detail performance and also solves issues with occasional artefacts on water reflections (2nd row, right-side buildings).

leverages the recently released TanDEM-X public Global Digital Elevation Model. Projected GDEM points represent scale depth anchors in the image frame that are then used to scale relative estimations, including those coming from scale- and shift-invariant models. Our adaptation for the Cloth Simulation Filter enables its use for segmenting ground pixels based on relative depth estimations and thus allows the scaling mechanism to be constrained to use only ground points.

The proposed system, when paired with modern relative MDE models, is shown to provide high-quality metric depth maps with good generalization performance across a variety of outdoor UAV scenes, including from the new UAVid-3D-Scenes dataset we develop for public release. TanDepth outperforms other types of online scale recovery methods, including the camera height-based method which we adapt to the aerial domain.

ACKNOWLEDGMENT

The OpenAI ChatGPT-40 LLM was used for grammar enhancement of selected phrases and for creating graphical elements in Fig. 1.

REFERENCES

- [1] F. Nex, C. Armenakis, M. Cramer, D. A. Cucci, M. Gerke, E. Honkavaara, A. Kukko, C. Persello, and J. Skaloud, "UAV in the advent of the twenties: Where we stand and what is next," *ISPRS journal of photogrammetry and remote sensing*, vol. 184, pp. 215–242, 2022.
- [2] M. A. Akhloufi, A. Couturier, and N. A. Castro, "Unmanned aerial vehicles for wildland fires: Sensing, perception, cooperation and assistance," *Drones*, vol. 5, no. 1, p. 15, 2021.
- [3] M. Lyu, Y. Zhao, C. Huang, and H. Huang, "Unmanned aerial vehicles for search and rescue: A survey," *Remote Sensing*, vol. 15, no. 13, p. 3266, 2023.
- [4] B. Mildenhall, P. P. Srinivasan, M. Tancik, J. T. Barron, R. Ramamoorthi, and R. Ng, "Nerf: Representing scenes as neural radiance fields for view synthesis," *Communications of the ACM*, vol. 65, no. 1, pp. 99–106, 2021.

- [5] R. Ranftl, K. Lasinger, D. Hafner, K. Schindler, and V. Koltun, "Towards robust monocular depth estimation: Mixing datasets for zero-shot crossdataset transfer," *IEEE transactions on pattern analysis and machine* intelligence, vol. 44, no. 3, pp. 1623–1637, 2020.
- [6] L. Yang, B. Kang, Z. Huang, X. Xu, J. Feng, and H. Zhao, "Depth anything: Unleashing the power of large-scale unlabeled data," arXiv preprint arXiv:2401.10891, 2024.
- [7] L. Yang, B. Kang, Z. Huang, Z. Zhao, X. Xu, J. Feng, and H. Zhao, "Depth anything V2," 2024. [Online]. Available: https://arxiv.org/abs/2406.09414
- [8] H. Florea and S. Nedevschi, "Survey on monocular depth estimation for unmanned aerial vehicles using deep learning," in 2022 IEEE 18th International Conference on Intelligent Computer Communication and Processing (ICCP). IEEE, 2022, pp. 319–326.
- [9] T. Zhou, M. Brown, N. Snavely, and D. G. Lowe, "Unsupervised learning of depth and ego-motion from video," in *Proceedings of the IEEE* conference on computer vision and pattern recognition, 2017, pp. 1851– 1858
- [10] P. Rizzoli, M. Martone, C. Gonzalez, C. Wecklich, D. B. Tridon, B. Bräutigam, M. Bachmann, D. Schulze, T. Fritz, M. Huber et al., "Generation and performance assessment of the global TanDEM-X digital elevation model," ISPRS Journal of Photogrammetry and Remote Sensing, vol. 132, pp. 119–139, 2017.
- [11] W. Zhang, J. Qi, P. Wan, H. Wang, D. Xie, X. Wang, and G. Yan, "An easy-to-use airborne LiDAR data filtering method based on cloth simulation," *Remote sensing*, vol. 8, no. 6, p. 501, 2016.
- [12] Y. Lyu, G. Vosselman, G.-S. Xia, A. Yilmaz, and M. Y. Yang, "UAVid: A semantic segmentation dataset for UAV imagery," *ISPRS journal of photogrammetry and remote sensing*, vol. 165, pp. 108–119, 2020.
- [13] V. Licăret, V. Robu, A. Marcu, D. Costea, E. Sluşanschi, R. Sukthankar, and M. Leordeanu, "Ufo depth: Unsupervised learning with flow-based odometry optimization for metric depth estimation," in 2022 International Conference on Robotics and Automation (ICRA). IEEE, 2022, pp. 6526–6532.
- [14] H. Florea, V.-C. Miclea, and S. Nedevschi, "WildUAV: Monocular UAV dataset for depth estimation tasks," in 2021 IEEE 17th International Conference on Intelligent Computer Communication and Processing (ICCP). IEEE, 2021, pp. 291–298.
- [15] R. Ranftl, A. Bochkovskiy, and V. Koltun, "Vision transformers for dense prediction," in *Proceedings of the IEEE/CVF international conference* on computer vision, 2021, pp. 12179–12188.
- [16] V. Guizilini, I. Vasiljevic, D. Chen, R. Ambruş, and A. Gaidon, "Towards zero-shot scale-aware monocular depth estimation," in *Proceedings of* the IEEE/CVF International Conference on Computer Vision, 2023, pp. 9233–9243.
- [17] L. Piccinelli, Y.-H. Yang, C. Sakaridis, M. Segu, S. Li, L. Van Gool, and F. Yu, "UniDepth: Universal monocular metric depth estimation," arXiv preprint arXiv:2403.18913, 2024.
- [18] H. Fu, M. Gong, C. Wang, K. Batmanghelich, and D. Tao, "Deep ordinal regression network for monocular depth estimation," in *Proceedings of* the IEEE conference on computer vision and pattern recognition, 2018, pp. 2002–2011.
- [19] S. F. Bhat, I. Alhashim, and P. Wonka, "Adabins: Depth estimation using adaptive bins," in *Proceedings of the IEEE/CVF conference on computer* vision and pattern recognition, 2021, pp. 4009–4018.
- [20] —, "Localbins: Improving depth estimation by learning local distributions," in *European Conference on Computer Vision*. Springer, 2022, pp. 480–496.
- [21] S. F. Bhat, R. Birkl, D. Wofk, P. Wonka, and M. Müller, "Zoedepth: Zero-shot transfer by combining relative and metric depth," arXiv preprint arXiv:2302.12288, 2023.
- [22] V.-C. Miclea and S. Nedevschi, "Monocular depth estimation with improved long-range accuracy for UAV environment perception," *IEEE Transactions on Geoscience and Remote Sensing*, vol. 60, pp. 1–15, 2021.
- [23] —, "Dynamic semantically guided monocular depth estimation for uav environment perception," *IEEE Transactions on Geoscience and Remote Sensing*, 2023.
- [24] L. Madhuanand, F. Nex, M. Yang, N. Paparoditis, C. Mallet, F. Lafarge, F. Remondino, I. Toschi, T. Fuse et al., "Deep learning for monocular depth estimation from UAV images," ISPRS Annals of the Photogrammetry, Remote Sensing and Spatial Information Sciences, vol. 2, 2020.
- [25] M. Fonder, D. Ernst, and M. Van Droogenbroeck, "M4depth: A motion-based approach for monocular depth estimation on video sequences," arXiv preprint arXiv:2105.09847, 2021.

- [26] R. Garg, V. K. Bg, G. Carneiro, and I. Reid, "Unsupervised cnn for single view depth estimation: Geometry to the rescue," in *European* conference on computer vision. Springer, 2016, pp. 740–756.
- [27] C. Godard, O. Mac Aodha, M. Firman, and G. J. Brostow, "Digging into self-supervised monocular depth estimation," in *Proceedings of* the IEEE/CVF International Conference on Computer Vision, 2019, pp. 3828–3838.
- [28] J.-W. Bian, H. Zhan, N. Wang, Z. Li, L. Zhang, C. Shen, M.-M. Cheng, and I. Reid, "Unsupervised scale-consistent depth learning from video," *International Journal of Computer Vision*, pp. 1–17, 2021.
- [29] L. Madhuanand, F. Nex, and M. Y. Yang, "Self-supervised monocular depth estimation from oblique UAV videos," *ISPRS journal of photogram*metry and remote sensing, vol. 176, pp. 1–14, 2021.
- [30] M. Hermann, B. Ruf, and M. Weinmann, "Real-time dense 3D reconstruction from monocular video data captured by low-cost UAVs," arXiv preprint arXiv:2104.10515, 2021.
- [31] F. Xue, G. Zhuo, Z. Huang, W. Fu, Z. Wu, and M. H. Ang, "Toward hierarchical self-supervised monocular absolute depth estimation for autonomous driving applications," in 2020 IEEE/RSJ International Conference on Intelligent Robots and Systems (IROS). IEEE, 2020, pp. 2330–2337.
- [32] B. Wagstaff and J. Kelly, "Self-supervised scale recovery for monocular depth and egomotion estimation," arXiv preprint arXiv:2009.03787, 2020.
- [33] H. Li, Y. Ma, Y. Gu, K. Hu, Y. Liu, and X. Zuo, "RadarCam-Depth: Radar-camera fusion for depth estimation with learned metric scale," arXiv preprint arXiv:2401.04325, 2024.
- [34] V. Guizilini, R. Ambrus, S. Pillai, A. Raventos, and A. Gaidon, "3d packing for self-supervised monocular depth estimation," in *Proceedings of the IEEE/CVF Conference on Computer Vision and Pattern Recognition*, 2020, pp. 2485–2494.
- [35] K. Swami, A. Muduli, U. Gurram, and P. Bajpai, "Do what you can, with what you have: Scale-aware and high quality monocular depth estimation without real world labels," in *Proceedings of the IEEE/CVF Conference* on Computer Vision and Pattern Recognition, 2022, pp. 988–997.
- [36] M. Pirvu, V. Robu, V. Licaret, D. Costea, A. Marcu, E. Slusanschi, R. Sukthankar, and M. Leordeanu, "Depth distillation: unsupervised metric depth estimation for UAVs by finding consensus between kinematics, optical flow and deep learning," in *Proceedings of the IEEE/CVF Conference on Computer Vision and Pattern Recognition*, 2021, pp. 3215–3223.
- [37] Y. Pan, B. Liu, Z. Liu, H. Shen, J. Xu, W. Fu, and T. Yang, "MoNA Bench: A benchmark for monocular depth estimation in navigation of autonomous unmanned aircraft system," *Drones*, vol. 8, no. 2, 2024. [Online]. Available: https://www.mdpi.com/2504-446X/8/2/66
- [38] T. G. Farr and M. Kobrick, "Shuttle Radar Topography Mission produces a wealth of data," *Eos, Transactions American Geophysical Union*, vol. 81, no. 48, pp. 583–585, 2000.
- [39] T. Tachikawa, M. Kaku, A. Iwasaki, D. B. Gesch, M. J. Oimoen, Z. Zhang, J. J. Danielson, T. Krieger, B. Curtis, J. Haase *et al.*, "ASTER global digital elevation model version 2-summary of validation results," NASA, Tech. Rep., 2011.
- [40] T. Tadono, H. Ishida, F. Oda, S. Naito, K. Minakawa, and H. Iwamoto, "Precise global DEM generation by ALOS PRISM," ISPRS Annals of the Photogrammetry, Remote Sensing and Spatial Information Sciences, vol. 2, pp. 71–76, 2014.
- [41] S. Shah, D. Dey, C. Lovett, and A. Kapoor, "Airsim: High-fidelity visual and physical simulation for autonomous vehicles," in *Field and service* robotics. Springer, 2018, pp. 621–635.
- [42] M. Fonder and M. Van Droogenbroeck, "Mid-air: A multi-modal dataset for extremely low altitude drone flights," in *Proceedings of the IEEE/CVF* conference on computer vision and pattern recognition workshops, 2019, pp. 0–0.
- [43] W. Wang, D. Zhu, X. Wang, Y. Hu, Y. Qiu, C. Wang, Y. Hu, A. Kapoor, and S. Scherer, "TartanAir: A dataset to push the limits of visual SLAM," in 2020 IEEE/RSJ International Conference on Intelligent Robots and Systems (IROS), 2020.
- [44] M. Hermann, M. Weinmann, F. Nex, E. Stathopoulou, F. Remondino, B. Jutzi, and B. Ruf, "Depth estimation and 3D reconstruction from UAV-borne imagery: Evaluation on the UseGeo dataset," ISPRS Open Journal of Photogrammetry and Remote Sensing, p. 100065, 2024.
- [45] J. Bian, Z. Li, N. Wang, H. Zhan, C. Shen, M.-M. Cheng, and I. Reid, "Unsupervised scale-consistent depth and ego-motion learning from monocular video," *Advances in neural information processing systems*, vol. 32, pp. 35–45, 2019.
- [46] QGIS Development Team, QGIS Geographic Information System, QGIS Association, 2024. [Online]. Available: https://www.qgis.org

- [47] GPL software, CloudCompare (version 2.13), 2024. [Online]. Available: http://www.cloudcompare.org
- [48] S. Katz, A. Tal, and R. Basri, "Direct visibility of point sets," in ACM SIGGRAPH 2007 papers, 2007, pp. 24–es.
- [49] B. Wessel, M. Huber, C. Wohlfart, U. Marschalk, D. Kosmann, and A. Roth, "Accuracy assessment of the global TanDEM-X digital elevation model with GPS data," *ISPRS Journal of Photogrammetry and Remote Sensing*, vol. 139, pp. 171–182, 2018.
- [50] J. L. Schönberger and J.-M. Frahm, "Structure-from-Motion Revisited," in Conference on Computer Vision and Pattern Recognition (CVPR), 2016.
- [51] J. L. Schönberger, E. Zheng, M. Pollefeys, and J.-M. Frahm, "Pixelwise View Selection for Unstructured Multi-View Stereo," in *European Conference on Computer Vision (ECCV)*, 2016.